Mineralogical Magazine, December 2017, Vol. 81(6), pp. 1533–1550

From structure topology to chemical composition. XXIII. Revision of the crystal structure and chemical formula of zvyaginite, $Na_2ZnTiNb_2(Si_2O_7)_2O_2(OH)_2(H_2O)_4$, a seidozerite-supergroup mineral from the Lovozero alkaline massif, Kola peninsula, Russia

E. Sokolova[1,*], A. Genovese[2], A. Falqui[2], F.C. Hawthorne[1] and F. Cámara[3]

[1] Department of Geological Sciences, University of Manitoba, 125 Dysart Road, Winnipeg, MB, R3T 2N2 Canada
[2] Biological and Environmental Sciences and Engineering Division, King Abdullah University of Science and Technology, Bldg. 2, Thuwal, 23955-6900, Saudi Arabia
[3] Dipartimento di Scienze della Terra "Ardito Desio", Università degli Studi di Milano, Via Mangiagalli 34, 20133, Milano, Italy

[*Received 9 November 2016; Accepted 21 February 2017; Associate Editor: Peter Leverett*]

ABSTRACT

The crystal structure and chemical formula of zvyaginite, ideally $Na_2ZnTiNb_2(Si_2O_7)_2O_2(OH)_2(H_2O)_4$, a lamprophyllite-group mineral of the seidozerite supergroup from the type locality, Mt. Malyi Punkaruaiv, Lovozero alkaline massif, Kola Peninsula, Russia have been revised. The crystal structure was refined with a new origin in space group $C\bar{1}$, $a = 10.769(2)$, $b = 14.276(3)$, $c = 12.101(2)$ Å, $\alpha = 105.45(3)$, $\beta = 95.17(3)$, $\gamma = 90.04(3)°$, $V = 1785.3(3.2)$ Å^3, $R_1 = 9.23\%$. The electron-microprobe analysis gave the following empirical formula [calculated on 22 (O + F)]: $(Na_{0.75}Ca_{0.09}K_{0.04}\square_{1.12})_{\Sigma 2}(Na_{1.12}Zn_{0.88}Mn_{0.17}Fe^{2+}_{0.04}\square_{0.79})_{\Sigma 3}(Nb_{1.68}Ti_{1.25}Al_{0.07})_{\Sigma 3}(Si_{4.03}O_{14})O_2[(OH)_{1.11}F_{0.89}]_{\Sigma 2}(H_2O)_4$, $Z = 4$. Electron-diffraction patterns have prominent streaking along **c*** and HRTEM images show an intergrowth of crystalline zvyaginite with two distinct phases, both of which are partially amorphous. The crystal structure of zvyaginite is an array of TS (Titanium-Silicate) blocks connected via hydrogen bonds between H_2O groups. The TS block consists of HOH sheets (H = heteropolyhedral, O = octahedral) parallel to (001). In the O sheet, the $^{[6]}M^{O}(1,4,5)$ sites are occupied mainly by Ti, Zn and Na and the $^{[6]}M^{O}(2,3)$ sites are occupied by Na at less than 50%. In the H sheet, the $^{[6]}M^{H}(1,2)$ sites are occupied mainly by Nb and the $^{[8]}A^{P}(1)$ and $^{[8]}A^{P}(2)$ sites are occupied mainly by Na and □. The M^H and A^P polyhedra and Si_2O_7 groups constitute the H sheet. The ideal structural formula is $Na\square Nb_2NaZn\square Ti(Si_2O_7)_2O_2(OH)_2(H_2O)_4$. Zvyaginite is a Zn-bearing and Na-poor analogue of epistolite, ideally $(Na\square)Nb_2Na_3Ti(Si_2O_7)_2O_2(OH)_2(H_2O)_4$. Epistolite and zvyaginite are related by the following substitution in the O sheet of the TS-block: $(Na^{+}_2)_{epi} \leftrightarrow Zn^{2+}_{zvy} + \square_{zvy}$. The doubling of the t_1 and t_2 translations of zvyaginite relative to those of epistolite is due to the order of Zn and Na along **a** ($\mathbf{t_1}$) and **b** ($\mathbf{t_2}$) in the O sheet of zvyaginite.

Keywords: zvyaginite, crystal-structure refinement, HRTEM, electron diffraction, EMP analysis, chemical formula, lamprophyllite group, seidozerite supergroup, TS-block minerals, epistolite.

Introduction

Zvyaginite was described from the Lovozero alkaline massif, Kola Peninsula, Russia by Pekov *et al.* (2014). They reported *a* structural model for

*E-mail: elena_sokolova@umanitoba.ca
https://doi.org/10.1180/minmag.2017.081.015

zvyaginite: space group $P\bar{1}$, $a = 8.975(3)$, $b = 8.979(3)$, $c = 12.135(4)$ Å, $\alpha = 74.328(9)$, $\beta = 80.651(8)$, $\gamma = 73.959(8)°$, $V = 900.8(6)$ Å^3, $R_1 = 15.9\%$ and gave the simplified and idealized formulae as $NaZnNb_2Ti(Si_2O_7)_2O(OH,F)_3(H_2O)_{4+x}$ ($x < 1$) and $NaZnNb_2Ti(Si_2O_7)_2O(OH)_3(H_2O)_4$, $Z = 2$. They stated that zvyaginite and epistolite [ideally $(Na\square)Nb_2Na_3Ti(Si_2O_7)_2O_2(OH)_2(H_2O)_4$, space group $P\bar{1}$, $a = 5.460(1)$, $b = 7.170(1)$, $c = 12.041(2)$ A, $\alpha = 103.63(3)$, $\beta = 96.01(3)$, $\gamma = 89.98(3)°$, $V = 455.4(5)$ Å^3, $R_1 = 9.8\%$, Sokolova and Hawthorne (2004)] are topologically identical but differ in composition of the O sheet in the HOH block, where partial substitution of Zn^{2+} for Na^+ occurs.

Zvyaginite and epistolite are lamprophyllite-group minerals of the seidozerite supergroup (Sokolova and Cámara, 2017). The forty-five seidozerite-supergroup minerals have structures based on a TS-block (TS = Titanium-Silicate). The TS-block consists of HOH sheets (H = heteropolyhedral, O = octahedral) and is characterized by a planar cell based on translation vectors, t_1 and t_2, with $t_1 \approx 5.5$ and $t_2 \approx 7$ Å and $t_1 \wedge t_2$ close to 90° (Sokolova, 2006; Sokolova and Cámara, 2013, 2016). The seidozerite-supergroup minerals are divided into four groups based on the content of Ti (+ Nb + Zr + Fe^{3+} + Mg + Mn), topology, chemical composition and stereochemistry of the TS block: rinkite group: Ti = 1 apfu (atoms per formula unit); bafertisite group: Ti = 2 apfu; lamprophyllite group: Ti = 3 apfu; murmanite group: Ti = 4 apfu. The four groups correspond to Groups I, II, III and IV of Sokolova (2006).

Ideal structural formulae of the lamprophyllite-group minerals with basic structures are given in Table 1. The lamprophyllite-group minerals with derivative structures: bornemanite (Cámara and Sokolova, 2007), nechelyustovite (Cámara and Sokolova, 2009), kazanskyite (Cámara *et al.*, 2012) and saamite (Cámara *et al.*, 2014) are not listed in the Table 1 as their structures are combination of structural fragments of basic structures of the lamprophyllite group [for the definition of basic and derivative structures see Sokolova and Cámara (2013)].

We considered the crystal structure of zvyaginite (Pekov *et al.*, 2014) and found some unresolved problems: (1) Their empirical formula, $Na_{1.24}K_{0.04}Ca_{0.11}Mn_{0.16}Al_{0.06}Fe_{0.03}Zn_{0.96}Nb_{1.66}Ti_{1.25}(Si_{3.97}Al_{0.03})_{\Sigma 4}O_{15.07}(OH)_{2.10}F_{0.83}(H_2O)_{4.64}$ (Table 2), gives $(H_2O)_{4.64}$ (Σanions = 22.64 apfu) and the structure-refinement results give $(H_2O)_4$ (Σanions = 22.00 apfu); hence there is significant disagreement between the chemical analysis and the structure-refinement results. (2) Aspects of the structure-refinement results raised questions about the correctness of the crystal-structure model: (*a*) ratios of U_{eq} for cations at the *Nb*(1) and *Nb*(2) sites and *Zn*(1) and *Zn*(2) sites were 3:1 and 1:3, respectively (Table 3); (*b*) Some interatomic distances were too long, e.g. $^{[6]}$Zn(2)–O(6) = 2.88 Å. (3) No quantitative relation between zvyaginite and epistolite was suggested.

We have re-examined zvyaginite as we wish to (1) relate epistolite and zvyaginite via the substitution mechanism in a quantitative way, and (2) understand the doubling of the t_1 and t_2 translations.

The forty-three TS-block structures of the seidozerite supergroup have unit cells based on translation vectors, $\mathbf{t_1}$ and $\mathbf{t_2}$ (Sokolova and Cámara, 2017), and only two structures, zvyaginite (Pekov *et al.*, 2014) and vigrishinite, $Zn_2Ti_{4-x}(Si_2O_7)_2O_2(OH,F,O)_2(H_2O,OH,\square)_4$, $x < 1$ (Pekov *et al.*, 2013; Lykova *et al.*, 2015), have unit cells based on the two diagonals of the planar cell: $\mathbf{a}_{zvy} = -\mathbf{t_1} + \mathbf{t_2}$ and $\mathbf{b}_{zvy} = \mathbf{t_1} + \mathbf{t_2}$. Such description of the crystal structure of zvyaginite complicates comparison of zvyaginite to epistolite (see the unit cell of epistolite above) and other TS-block structures.

Here, we report revision of the crystal structure of zvyaginite with a different origin and the refinement of the structure in space group $C\bar{1}$ for better comparison with all other TS-block structures; we will explain doubling of the t_1 and t_2 translations of zvyaginite relative to those translations in epistolite and revise the chemical formula of zvyaginite.

Description of the sample

Sample description

We obtained several fragments of a zvyaginite sample from an American mineral collector. This sample comes from the type locality, Mt. Malyi Punkaruaiv, Lovozero alkaline massif, Kola Peninsula, Russia (Pekov *et al.*, 2014). From those fragments, we extracted five crystals for which we collected single-crystal X-ray data. Based on the unit-cell parameters, three crystals were identified as zvyaginite and two crystals as vigrishinite. The three crystals of zvyaginite are transparent colorless thin plates. In this paper, we report the structure solution and refinement results for crystal #3; crystal #2 of zvyaginite was used for the microprobe analysis.

https://doi.org/10.1180/minmag.2017.081.015 Published online by Cambridge University Press

TABLE 1. Ideal structural formulae of the lamprophyllite-group minerals* (seidozerite supergroup) with basic structures.

Mineral	Str. type**	Ideal structural formula										Space group	Z	Ref.†
		A_2^P	B_2^P	M_2^H	M_4^O		$(Si_2O_7)_2$		$(X_M^O)_2$	$(X_A^O)_2$	$(X_{M,A}^P)_4$			
Lamprophyllite-2*M*, -2*O*	B1(LG)	(SrNa)		$^{[5]}\mathbf{Ti_2}$	$\mathbf{Na_3}$	**Ti**	$(Si_2O_7)_2$		$\mathbf{O_2}$	$\mathbf{(OH)_2}$		*C*2/*m*, *Pnmn*	2	(1)
Fluorlamprophyllite	B1(LG)	(SrNa)		$^{[5]}\mathbf{Ti_2}$	$\mathbf{Na_3}$	**Ti**	$(Si_2O_7)_2$		$\mathbf{O_2}$	$\mathbf{F_2}$		*C*2/*m*	2	(2)
Nabalamprophyllite-2*M*	B1(LG)	BaNa		$^{[5]}\mathbf{Ti_2}$	$\mathbf{Na_3}$	**Ti**	$(Si_2O_7)_2$		$\mathbf{O_2}$	$\mathbf{(OH)_2}$		*P*2/*m*	2	(3)
Nabalamprophyllite-2*O*	B1(LG)	(BaNa)		$^{[5]}\mathbf{Ti_2}$	$\mathbf{Na_3}$	**Ti**	$(Si_2O_7)_2$		$\mathbf{O_2}$	$\mathbf{(OH)_2}$		*Pnmn*	2	(4)
Barytolamprophyllite	B1(LG)	(BaK)		$^{[5]}\mathbf{Ti_2}$	$\mathbf{Na_3}$	**Ti**	$(Si_2O_7)_2$		$\mathbf{O_2}$	$\mathbf{(OH)_2}$		*C*2/*m*	2	(5)
Lileyite***	B1(LG)	Ba_2		$^{[5]}\mathbf{Ti_2}$	$\mathbf{Na(NaM^{2+})}$	**Mg**	$(Si_2O_7)_2$		$\mathbf{O_2}$	$\mathbf{F_2}$		*C*2/*m*	2	(6)
Emmerichite	B1(LG)	Ba_2		$^{[5]}\mathbf{Ti_2}$	$\mathbf{Na_3}$	$\mathbf{Fe^{3+}}$	$(Si_2O_7)_2$		$\mathbf{O_2}$	$\mathbf{F_2}$		*C*2/*m*	2	(7)
Innelite-1*A*, -2*M****	B2(LG)	Ba_2	Ba_2	$^{[5]}\mathbf{Ti_2}$	$\mathbf{Na(NaM^{2+})}$	**Ti**	$(Si_2O_7)_2$	$[(SO_4)\,(PO_4)]$	$\mathbf{O_2}$	**[O(OH)]**		$P\bar{1}$, *P*2/*c*	1,2	(8)
Epistolite	B3(LG)	(Na□)		$^{[6]}\mathbf{Nb_2}$	$\mathbf{Na_3}$	**Ti**	$(Si_2O_7)_2$		$\mathbf{O_2}$	$\mathbf{(OH)_2}$	$(H_2O)_4$	$P\bar{1}$	1	(9)
Zvyaginite	B3(LG)	Na□		$^{[6]}\mathbf{Nb_2}$	$\mathbf{ZnNa□}$	**Ti**	$(Si_2O_7)_2$		$\mathbf{O_2}$	$\mathbf{(OH)_2}$	$(H_2O)_4$	$C\bar{1}$	4	(10)
Vuonnemite	B4(LG)	Na_6 Na_2		$^{[6]}\mathbf{Nb_2}$	$\mathbf{Na_3}$	**Ti**	$(Si_2O_7)_2$	$(PO_4)_2$	$\mathbf{O_2}$	**(OF)**		$P\bar{1}$	1	(11)
Delindeite****	Related	Ba_2		$^{[6]}\mathbf{Ti_2}$	$\mathbf{(Na_2□)}$	**Ti**	$(Si_2O_7)_2$		$\mathbf{(OH)_2}$	$\mathbf{(H_2O)_2}$	O_2	*C*2/*c*	8	(12)

***Ti (+Nb + Fe^{3+} + Mg) = 3 apfu.**

Structure type: B (basic) (Sokolova and Cámara, 2013); LG = Lamprophyllite group. The invariant core of the TS block, $\mathbf{M_2^H M_4^O (Si_2O_7)_2 X_4^O}$, is shown in bold; M^O and M^H = cations of the O and H sheets, A^P and B^P = cations at the peripheral (*P*) sites; X_4^O = anions of the O sheet not bonded to Si: X_M^O = anions at the common vertices of $3M^O$ and M^H polyhedra; X_A^O = anions at the common vertices of $3M^O$ and A^P polyhedra (where A^P–X_A^O < 3 Å); X_M^P and X_A^P = apical anions of M^H and A^P cations at the periphery of the TS block. In the lamprophyllite group, A^P and B^P cations (except for Na atoms which occur in the plane of the H sheet), plus Na atoms and (PO_4) groups (vuonnemite) and $[(PO_4)(SO_4)]$ groups (innelite) constitute the **I block (shown in turquoise colour).

*** M^{2+} = Fe^{2+}, Ca, Mn (lileyite); M^{2+} = Mn, Fe^{2+}, Mg, Ca (innelite).

****Due to the Na-H_2O disorder in the O sheet, the TS block in delindeite retains linkage 1 but exhibits stereochemistry of the rinkite group.

† The most recent reference on the structure: (1) Krivovichev *et al.* (2003); (2) Andrade *et al.* (2017); (3) Rastsvetaeva and Chukanov (1999); (4) Sokolova and Hawthorne (2008); (5) Sokolova and Cámara (2008); (6) Chukanov *et al.* (2012); (7) Aksenov *et al.* (2014); (8) Sokolova *et al.* (2011); (9) Sokolova and Hawthorne (2004); (10) this work; (11) Ercit *et al.* (1998); (12) Sokolova and Cámara (2007).

TABLE 2. Chemical composition and unit formula for zvyaginite.

Chemical composition* (wt.%)				Unit formula (apfu)***	
	This work	Pekov *et al.* (2014)		This work	Pekov *et al.* (2014)
Nb_2O_5	27.33	27.72	Nb	1.68	1.66
TiO_2	12.23	12.33	Ti	1.25	1.25
SiO_2	29.63	29.42	Si	4.03	3.97
Al_2O_3	0.42	0.19	Al	0.07	0.03
ZnO	8.71	9.61	Zn	0.88	0.96
FeO	0.34	0.24	Fe^{2+}	0.04	0.03
MnO	1.44	1.36	Mn	0.17	0.16
CaO	0.59	0.77	Ca	0.09	0.11
K_2O	0.25	0.22	K	0.04	0.04
Na_2O	**7.10**	**4.74**	**Na**	**1.87**	**1.24**
F	2.06	1.94	F	0.89	0.83
H_2O	10.04*	12.65**	OH	1.11	2.10
O = F	–0.87	–0.82	H_2O	4.00	4.64
Total	99.27	99.87	Σcations	10.12	9.45
			Σ(anions, H_2O gr.)	22.00	22.64

*Calculated from crystal-structure refinement.
**Modified Penfield method.
***Formula calculated on: (1) this work: 22 (O + F) apfu, with OH + F = 2 pfu and H_2O = 4 pfu; and (2) Pekov *et al.* (2014): Si + Al = 8 apfu.

Transmission electron microscopy (TEM)

We prepared three different zvyaginite samples 2–3 mm in width for transmission electron microscopy (TEM) by selecting crystals with evident {001} cleavage and well-developed lateral crystal faces, useful for approximate pre-orientation along the main lattice vectors. Each pre-oriented crystal was sandwiched and glued between two graphite supports, and after that underwent both mechanical and ion polishing to obtain a thin and electron-transparent section.

The high-resolution TEM (HRTEM) images and electron-diffraction (ED) patterns were acquired using an FEI Titan Cubed 60–300 electron microscope equipped with a high-brightness field emission gun, a Wien-type monochromator, a spherical-aberration (Cs) corrector for the objective lens system allowing atomic spatial resolution (0.9 Å), a Gatan K2-IS direct-detection camera

TABLE 3. Refined site-scattering, assigned site-populations and U_{eq} for cation sites (excluding *Si*) in zvyaginite after Pekov *et al.* (2014).

Site	Mult.*	Refined site-scattering (epfu)	Assigned site-population (apfu)	U_{eq} (Å^2)
Nb(1)	1.0	32.6	$Nb_{0.56}Ti_{0.44}$	0.029
Nb(2)	1.0	41.0	Nb	0.010
Ti(1)	0.5	10.0	$Ti_{0.455}\square_{0.045}$	0.014
Ti(2)	0.5	11.1	$Ti_{0.505}$	0.016
Zn(1)	1.0	22.8	$Zn_{0.58}\square_{0.42}$	0.007
Zn(2)	1.0	24.8	$Zn_{0.62}\square_{0.38}$	0.023
Na(1)	1.0	5.1	$Na_{0.46}\square_{0.54}$	0.023
Na(2)	1.0	5.4	$Na_{0.49}\square_{0.51}$	0.026
Na(3)	1.0	5.3	$Na_{0.48}\square_{0.52}$	0.027

* Multiplicity, space group $P\bar{1}$.

https://doi.org/10.1180/minmag.2017.081.015 Published online by Cambridge University Press

with a 14.2-megapixel sensor able to sample images at rates up to 1600 full frames per second, and a post-column Gatan Image Filter (GIF) Tridiem 865.

All thin crystalline sections were coated with a thin layer of carbon a few nanometres thick to prevent local charging and dissipate heat during the TEM observations. The HRTEM imaging was done at 300 kV tuning the Cs corrector with a negative Cs value (–15 μm) to maximize spatial resolution and the contrast of the atomic columns, respectively, in low-dose conditions (~50 e^{-}/Å^{2}s) to limit beam damage of the crystals, and using the direct-detection camera to maximize the signal-to-noise ratio. The Cs corrector allows collection of a vast extension of lattice frequencies – up to 11.1 nm^{-1} in reciprocal units – without reversals in the contrast transfer function (CTF), and extending the final resolution up to the information limit of the lens system. This advantage eliminates the need of objective apertures for HRTEM imaging. In particular, during the TEM analysis, the three samples were oriented correctly along the zone axes.

Zvyaginite thin sections exhibited feeble electron-beam damage despite the precautions taken for a correct and safe TEM imaging.

The TEM investigation of the samples revealed a band structure characterized by the alternation of defect-free bands and defective domains along the <001> direction. The defect-bearing bands, in turn, exhibited interleaving of {001} lamellae extended many hundreds of nanometres along the <110> direction, a few tens of nanometres along the <001> but very few tens of nanometres along the <$\bar{1}$10> direction.

The [00$\bar{1}$] projection

HRTEM imaging along the [00$\bar{1}$] zone axis showed large undisturbed regions of the crystal. The corresponding ED patterns contained **g**($\bar{1}$10) and **g**(110) reciprocal crystal directions forming an angle of 104°, but with no evidence of twinning or apparent streaking along these directions (Fig. 1*a*). The [00$\bar{1}$] diffraction features may be a direct indication of such a lamellar structure for zvyaginite, where {001} defect-rich domains are separated by extended and undisturbed crystal regions.

The lattice geometry characterization, extrapolated from Fourier-transform (FT) pattern analysis and direct-space imaging, shows planar (2D) cells with rhombic symmetry forming angles of ~76° and ~104°. The corresponding interplanar spacings are $d(\bar{1}10) \approx 8.6$ Å and $d(110) \approx 8.3$ Å, in accord with the triclinic structure of zvyaginite described by the $\mathbf{t_1}$ and $\mathbf{t_2}$ translational vectors and the space group $C\bar{1}$ (Fig. 1*b*).

The [110] projection

Similarly, HRTEM investigation of crystal sections along the [110] zone axis also shows the presence of large and undisturbed domains. The corresponding ED patterns show apparent **g**($\bar{1}$10) and **g**(00$\bar{1}$) reciprocal axes forming an angle of 95° (Fig. 2*a*). Again, there were no indications of any twinning or streaking along these main lattice directions, confirming the limited lateral width of the defective lamellae along the <$\bar{1}$10> direction. The high-magnification HRTEM image displays 2D lattice cells with a quasi-rhombic geometry and internal angles of ~85° and ~95°, with $d(\bar{1}10) \approx 8.6$ Å and $d(00\bar{1}) \approx 11.5$ Å (Fig. 2*b*).

The [1$\bar{1}$0] projection

The HRTEM images of zvyaginite along the [$\bar{1}$10] zone axis show a lamellar structure interleaved along the <001> direction. There are three different types of lamellae (type-I, type-II, type-III), on the basis of their electron contrast, crystallinity and internal structure, which alternate along the <001> direction. Type-I lamellae exhibit an even electron contrast and high-to-moderate crystallinity with a weak tendency to be amorphized on exposure to the electron-beam. These lamellae are directly related to the undisturbed zvyaginite structure. Type-II lamellae show a lighter electron contrast and scarce crystallinity that amorphizes completely during observation. Type-III lamellae display an electron contrast similar to type-I, but intermediate crystallinity due to a highly defective structure characterized by wavy and ill-defined lattice planes, which become amorphous under the beam (Fig. 3*a*).

The [$\bar{1}$10] ED patterns of zvyaginite thin sections display intense streaking along and parallel to the <001> direction, which can be ascribed to pervasive interleaving of {001} domains and their defective internal structure mainly due to the disorder in the heteropolyhedral sheets, which generate lamellae of different thickness and ion distribution. Electron diffraction indexing allowed straightforward identification of the **g**(110) and **g**(00$\bar{1}$) reciprocal axes, forming an angle of 104°, and the correct orientation of the lamellae with respect to the lattice vectors (Fig. 3*a*). The distribution of the three types of lamellae was not the same across the crystals: type-I and type-II

https://doi.org/10.1180/minmag.2017.081.015 Published online by Cambridge University Press

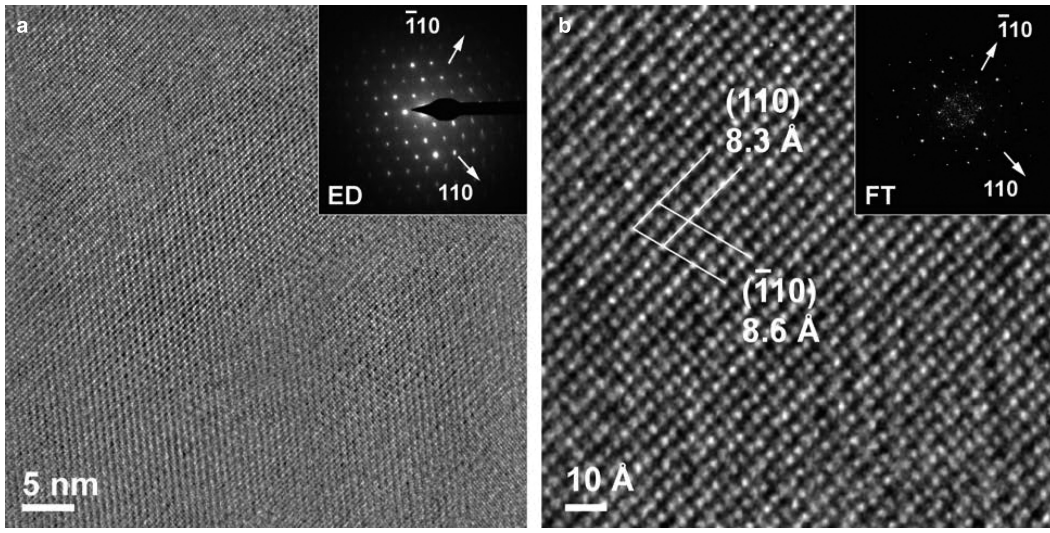

FIG. 1. HRTEM images of zvyaginite along the $[00\bar{1}]$ zone axis. (*a*) Intermediate magnification of an undisturbed region a few hundred nanometres across with its corresponding ED pattern showing $\mathbf{g}(\bar{1}10)$ and $\mathbf{g}(110)$ with no streaking. (*b*) Higher magnification showing a rhombic 2D lattice cell, as confirmed by the corresponding FT (inset); $d(\bar{1}10) \approx 8.6$ Å and $d(110) \approx 8.3$ Å.

lamellae are ubiquitous, but type-III are sporadic. The typical HRTEM image of the $[\bar{1}10]$ zone is shown in Fig. 3*b*, where only lamellae of type-I (darker electron contrast) and type-II (lighter electron contrast) can be identified.

Careful investigation of type-I lamellae revealed slight differences in their fine structure. A $[\bar{1}10]$ HRTEM image of the undisturbed fine structure of zvyaginite is displayed in Fig. 3*c*, where the uninterrupted lattice planes $d(110)$ ($\approx$ 8.3 Å) and

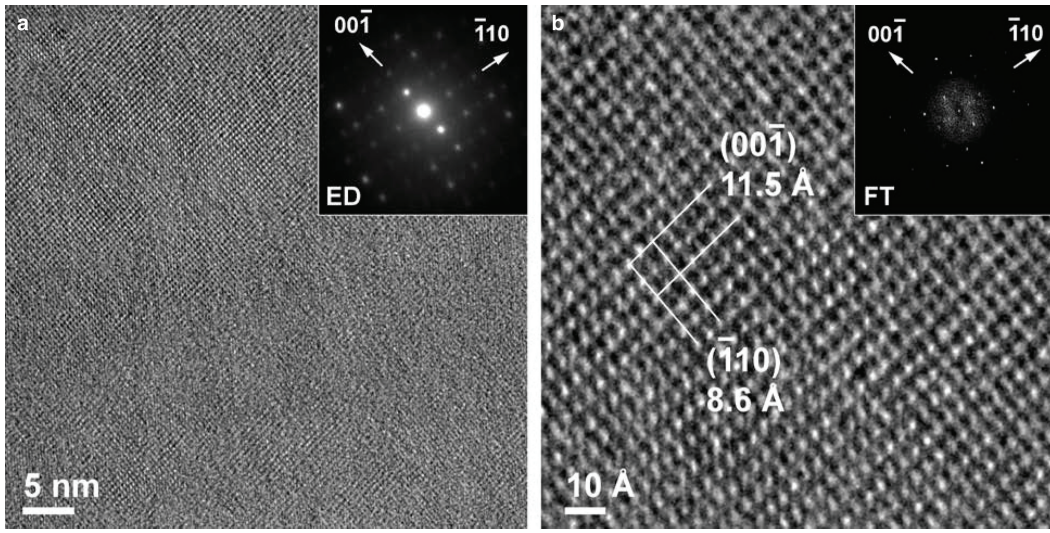

FIG. 2. HRTEM images of zvyaginite along the [110] zone axis. (*a*) Intermediate magnification of an undisturbed region a few hundred nanometres across with its corresponding ED pattern showing $\mathbf{g}(\bar{1}10)$ and $\mathbf{g}(00\bar{1})$ with no streaking. (*b*) Higher magnification showing quasi-rhombic 2D lattice cell, as shown in the corresponding FT (inset); $d(\bar{1}10) \approx 8.6$ Å and $d(00\bar{1}) \approx 11.5$ Å.

https://doi.org/10.1180/minmag.2017.081.015 Published online by Cambridge University Press

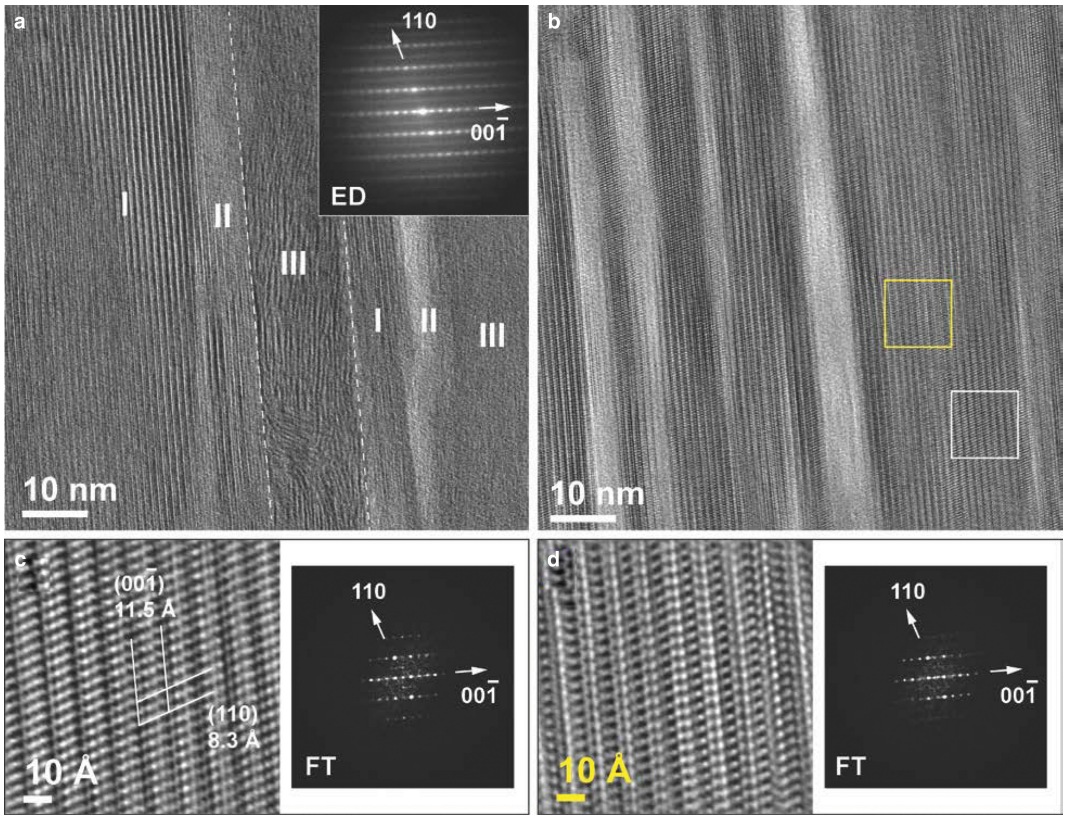

FIG. 3. HRTEM images of zvyaginite along the [$\bar{1}$10] zone axis. (*a*) HRTEM image at intermediate magnification showing the [00$\bar{1}$] stacking of the three types of lamellae (I, II, III); note the corresponding ED pattern (inset) showing **g**(110) and **g**(00$\bar{1}$) and intense streaking parallel to the [00$\bar{1}$] direction. (*b*) HRTEM image at intermediate magnification showing typical interleaving of type-I and type-II lamellae; white and yellow squares depict two regions of interest (ROI) within type-I lamella. (*c*) HRTEM detail of white ROI in (*b*), and corresponding FT (inset) showing the uninterrupted crystal structure with rhombic-shaped 2D lattice cell with $d(110) \approx 8.3$ Å and $d(00\bar{1}) \approx 11.5$ Å. (*d*) HRTEM detail of yellow ROI in (*b*), and corresponding FT (inset) showing a subtle change in the type-I lamella.

$d(00\bar{1})$ (≈11.5 Å) form rhombic-shaped 2D lattice cells with internal angles of ~76° and ~104°, as expected. However, a few tens of nanometres from the undisturbed regions, the fine structure of type-I lamellae exhibits a small but noticeable change that may be correlated with the stacking of layers with a slightly different structure along the <001> direction (Fig. 3*d*).

Chemical analysis

The crystal of zvyaginite used for the microprobe analysis is a plate (0.08 mm × 0.05 mm × 0.005 mm) where the edges have some curvature, and hence the data were collected in the central flat part of the plate. The crystal was analysed with a Cameca SX-100 electron-microprobe operating in wavelength-dispersion mode with an accelerating voltage of 15 kV, a specimen current of 5 nA, a beam size of 20 μm and count times on peak and background of 20 and 10 s, respectively. The following standards were used: Si, Ca: diopside; Al: andalusite; F: fluoribeckite; Na: albite; Nb: $Ba_2NaNb_5O_{15}$; Fe: fayalite; Mn: spessartine; Zn: gahnite; Ti: titanite; K: orthoclase. Ta, Zr, Mg and Sr were sought but not detected. Data were reduced using the φ(ρZ) procedure of Pouchou and Pichoir (1985). For Na_2O, 7.10 wt.% was achieved only for the first point and further attempts to analyse this grain again resulted in lower values for Na_2O, ~6.34–6.94, indicating diffusion of Na away from the

https://doi.org/10.1180/minmag.2017.081.015 Published online by Cambridge University Press

excitation volume of the electron beam. To calculate the empirical formula of zvyaginite in accord with the structure results, we used the Na_2O value from point 1. The chemical composition of zvyaginite is the mean of three determinations and is given in Table 2. Our chemical analysis of zvyaginite is close to that of Pekov *et al.* (2014) except for the higher Na_2O content 7.10 *vs.* 4.74 wt.% (Pekov *et al.*, 2014) (Table 2).

The empirical formula of zvyaginite was calculated on the basis of 22 (O + F) with two constraints derived from the crystal-structure refinement: (1) OH + F = 2 pfu and (2) H_2O = 4 pfu, giving $(Na_{0.75}Ca_{0.09}K_{0.04}\square_{1.12})_{\Sigma2}(Na_{1.12}Zn_{0.88}Mn_{0.17}Fe^{2+}_{0.04}\square_{0.79})_{\Sigma3}(Nb_{1.68}Ti_{1.25}Al_{0.07})_{\Sigma3}(Si_{4.03}O_{14})O_2[(OH)_{1.11}F_{0.89}]_{\Sigma2}(H_2O)_4$, $Z = 4$. The ideal formula is $Na_2ZnTiNb_2(Si_2O_7)_2O_2(OH)_2(H_2O)_4$.

TABLE 4. Miscellaneous refinement data for zvyaginite.

	(1)*	(2)**
a (Å)	10.769(2)	8.944(6)
b	14.276(3)	8.938(5)
c	12.101(2)	12.101(8)
α(°)	105.45(3)	74.516(9)
β	95.17(3)	80.89(1)
γ	90.04(3)	74.07(1)
V (Å^3)	1785.3(3.2)	892.7(1.6)
Refl. ($I_o > 10\sigma I$)	6840	6840
Space group	$C\bar{1}$	$P\bar{1}$
Z	4	2
Absorption coefficient (mm^{-1})	3.40	1.70
F(000)	1578.0	789.0
$D_{calc.}$ (g/cm^3)	3.02	3.02
Crystal size (mm)	0.120 × 0.060 × 0.004	
Radiation/monochromator	Mo*K*α/graphite	
$2\theta_{max}$ (°)	60.12	60.12
R(int) (%)	4.57	4.57
Reflections collected	10,111	10,111
Independent reflections	5101	5101
Reflections with $F_o > 4\sigma F$	3586	3587
Refinement method	Full-matrix least squares on F^2, fixed weights proportional to $1/\sigma F_o^2$	
Final $R_{(obs)}$ (%)		
R_1 [$F_o > 4\sigma F$]	9.23	9.42
R_1 (all data)	12.27	12.49
wR_2	23.68	24.32
Goodness of fit on F^2	1.089	1.083

* The two unit-cell parameters of zvyaginite (1) are doubled where compared to those of epistolite: $a_{zvy} = 2a_{epi}$; $b_{zvy} = 2b_{epi}$.
**The unit cell (2), space group $P\bar{1}$, is a reduced unit cell equivalent to the unit cell of zvyaginite of Pekov *et al.* (2014): *a* = 8.975(3), *b* = 8.979(3), *c* = 12.135(4) Å, α = 74.328(9), β = 80.651(8), γ = 73.959(8)°, *V* = 900.8(6) Å^3. To transform the unit cell (2) into the unit cell (1) we use matrix ($\bar{1}10$ 110 00$\bar{1}$).

X-ray data collection and structure refinement

We collected single-crystal X-ray data for zvyaginite crystals #1, #2 and #3 and refined their crystal structures using atom coordinates of Pekov *et al.* (2014) to R_1 = 15.78, 14.28 and 12.69%, respectively. However, we encountered the same problems that we outlined above: the ratios of U_{eq} for cations at the *Nb*(1) and *Nb*(2) sites and *Zn*(1) and *Zn*(2) sites were 3:1 and 1:3, respectively; $^{[6]}$Zn(2)–O(6) = 2.88 Å. We used direct methods to find another solution and were able to refine the structure in space group $P\bar{1}$ to R_1 = 9.42% (Table 4). Our new structure had a different origin when compared to the structure of Pekov *et al.* (2014) and was free of the problems outlined above. However we felt that the refinement of the structure of zvyaginite using a unit cell based on t_1 and t_2 translations would give us an opportunity to better understand the relation between zvyaginite and all other TS-block structures, especially epistolite. We used the transformation matrix ($\bar{1}10$ 110 00$\bar{1}$) to go from the unit cell of Pekov *et al.* (2014) to the unit cell based on t_1 and t_2 translations, space group $C\bar{1}$ (Table 4). The unit cell of Pekov *et al.* (2014) is a reduced cell with regard to the unit cell with space group $C\bar{1}$. Below we give details of data collection and structure refinement using the $C\bar{1}$ setting.

X-ray data for zvyaginite were collected for crystal #3 with a Bruker APEX II ULTRA three-circle diffractometer equipped with a rotating-anode generator (Mo*K*α), multilayer optics and an APEX II 4K CCD detector. Details of data collection and structure refinement are given in Table 4. The intensities of reflections with $-14 \le h \le 15$, $-19 \le k \le 19$, $-16 \le l \le 16$ were collected with a frame width of 0.5° and a frame time of 18 s, and an empirical absorption correction (*SADABS*, Sheldrick, 2008) was applied. The crystal structure of zvyaginite was solved and refined in space group $C\bar{1}$ with the Bruker *SHELXTL* Version 5.1 (*SADABS*, Sheldrick, 2008). The crystal structure of zvyaginite was refined to R_1 = 9.23% (Table 4). The occupancies of nine cation sites were refined with the following scattering curves: M^H(1,2) and A^P(1,2) sites: Nb and Na; M^O(1) site: Ti; M^O(2), M^O(3) and M^O(5) sites: Na; M^O(4) site: Zn. We

https://doi.org/10.1180/minmag.2017.081.015 Published online by Cambridge University Press

TABLE 5. Atom coordinates and equivalent displacement parameters (Å^2) for zvyaginite.

Atom	Site occ. (%)	x	y	z	U_{eq}
$M^H(1)$	100	0.89893(9)	0.18624(8)	0.74159(10)	0.0196(4)
$M^H(2)$	100	0.39831(9)	0.19855(8)	0.74170(10)	0.0183(4)
$M^O(1)$	100	0.25277(19)	0.00006(14)	0.0013(2)	0.0223(7)
$M^O(2)$	48	¼	¼	0	0.031(5)
$M^O(3)$	42	¾	¼	0	0.034(5)
$M^O(4)$	97	0.00009(13)	0.11964(10)	0.00036(15)	0.0199(5)
$M^O(5)$	79	0.4999(4)	0.1296(3)	–0.0001(3)	0.0346(14)
$A^P(1)$	64	0.3928(5)	0.9354(5)	0.7030(6)	0.027(2)
$A^P(2)$	24	0.108(2)	0.072(3)	0.300(3)	0.101(19)
Si(1)	100	0.1508(3)	0.8427(2)	0.7663(3)	0.0193(7)
Si(2)	100	0.1502(3)	0.0534(2)	0.7667(3)	0.0195(7)
Si(3)	100	0.1504(3)	0.3427(2)	0.7637(3)	0.0201(7)
Si(4)	100	0.3497(3)	0.9475(2)	0.2373(3)	0.0204(7)
O(1)	100	0.5235(7)	0.2853(6)	0.7115(8)	0.0303(19)
O(2)	100	0.7706(8)	0.2784(7)	0.7273(9)	0.037(2)
O(3)	100	0.1555(7)	0.8798(6)	0.9056(7)	0.0254(17)
O(4)	100	0.1602(8)	0.9367(5)	0.7140(8)	0.0281(18)
O(5)	100	0.2696(8)	0.0994(7)	0.7291(9)	0.037(2)
O(6)	100	0.0225(8)	0.0841(7)	0.7131(9)	0.037(2)
O(7)	100	0.1548(7)	0.0778(6)	0.9057(8)	0.0257(17)
O(8)	100	0.0222(8)	0.2810(7)	0.7272(9)	0.036(2)
O(9)	100	0.2675(8)	0.2842(7)	0.7108(9)	0.038(2)
O(10)	100	0.3264(8)	0.1187(6)	0.0975(8)	0.0286(18)
O(11)	100	0.3691(8)	0.0640(6)	0.2893(8)	0.0298(19)
O(12)	100	0.3262(8)	0.9244(6)	0.0992(8)	0.0281(18)
O(13)	100	0.5224(8)	0.0963(6)	0.7270(9)	0.037(2)
O(14)	100	0.7665(8)	0.0859(7)	0.7082(9)	0.040(2)
$X^O_M(1)$	100	0.9170(7)	0.2051(7)	0.8942(8)	0.032(2)
$X^O_M(2)$	100	0.4184(8)	0.2458(7)	0.8953(8)	0.034(2)
$X^O_A(1)$	100	0.3821(7)	0.9780(6)	0.9072(8)	0.0280(18)
$X^O_A(2)$	100	0.0986(7)	0.0199(6)	0.0888(7)	0.0226(16)
$X^P_M(1)$	100	0.8882(12)	0.1537(10)	0.5424(10)	0.056(3)
$X^P_M(2)$	100	0.3713(12)	0.1405(10)	0.5431(10)	0.059(3)
$X^P_A(1)$	100	0.3767(13)	0.8703(14)	0.5207(15)	0.090(5)
$X^P_A(2)$	24	0.125(5)	0.136(3)	0.483(5)	0.034(11)
W	76	0.1178(16)	0.1003(11)	0.4416(16)	0.041(4)
Subsidiary peaks					
$M^H(1A)$	1	0.911(6)	0.264(6)	0.896(7)	0.0196(4)
$M^H(1B)$	6	0.9018(15)	0.1325(16)	0.7389(17)	0.0196(4)
$M^H(2A)$	8	0.3969(10)	0.1402(9)	0.7403(11)	0.0183(4)

observed disorder of Na and □ (vacancy) at the $A^P(2)$ site and H_2O and □ at the W and $X^P_A(2)$ sites, with $A^P(2)$–W = 1.65 Å and $X^P_A(2)$–W = 0.61 Å. Scattering curves for neutral atoms were taken from the *International Tables for Crystallography* (Wilson, 1992). At the last stages of the refinement, three subsidiary peaks were included in the refinement (scattering curve of Nb); these are probably due to the presence of type-II and type-III lamellae intergrown with zvyaginite (Fig. 3). Final atom coordinates and equivalent displacement parameters are given in Table 5, selected interatomic distances and angles in Table 6, refined site-scattering values and assigned site-populations in Table 7, and bond-valence values for selected anions in Table 8. A list of observed and calculated structure factors, a Crystallographic Information File (CIF) and a table of anisotropic displacement parameters have been deposited with the Principal Editor of *Mineralogical Magazine* and are available from http://www.minersoc.org/pages/e_journals/dep_mat_mm.html

https://doi.org/10.1180/minmag.2017.081.015 Published online by Cambridge University Press

TABLE 6. Selected interatomic distances (Å) and angles (°) in zvyaginite.

$M^O(1)$–$X^O_A(1)$a	1.853(9)	$M^O(2)$–$X^O_M(2)$c	2.296(9) x2	$M^O(3)$–$X^O_M(1)$c	2.295(9) x2
$M^O(1)$–O(10)	1.907(9)	$M^O(2)$–O(10)	2.567(8) x2	$M^O(3)$–O(12)d	2.557(8) x2
$M^O(1)$–O(12)b	1.927(9)	$M^O(2)$–O(7)c	2.586(8) x2	$M^O(3)$–O(3)e	2.587(8) x2
$M^O(1)$–O(3)a	2.026(8)	<$M^O(2)$–O>	2.483	<$M^O(3)$–O>	2.479
$M^O(1)$–$X^O_A(2)$	2.029(8)				
$M^O(1)$–O(7)c	2.037(8)				
<$M^O(1)$–φ>	1.963				
$M^O(4)$–O(7)c	2.104(8)	$M^O(5)$–O(10)	2.32(1)	$M^H(1)$–$X^O_M(1)$	1.786(9)
$M^O(4)$–O(3)f	2.108(8)	$M^O(5)$–O(12)d	2.34(1)	$M^H(1)$–O(2)	1.937(9)
$M^O(4)$–$X^O_M(2)$g	2.136(9)	$M^O(5)$–$X^O_A(1)$e	2.43(1)	$M^H(1)$–O(8)k	1.946(9)
$M^O(4)$–$X^O_M(1)$h	2.137(9)	$M^O(5)$–$X^O_A(1)$a	2.45(1)	$M^H(1)$–O(6)k	1.958(8)
$M^O(4)$–$X^O_A(2)$	2.215(8)	$M^O(5)$–$X^O_M(2)$c	2.46(1)	$M^H(1)$–O(14)	1.959(8)
$M^O(4)$–$X^O_A(2)$i	2.215(8)	$M^O(5)$–$X^O_M(1)$j	2.49(1)	$M^H(1)$–$X^P_M(1)$	2.32(1)
<$M^O(4)$–φ>	2.153	<$M^O(5)$–φ>	2.42	<$M^H(1)$–φ>	1.984
$M^H(2)$–$X^O_M(2)$	1.794(9)	$A^P(1)$–$X^P_A(1)$	2.15(2)	$A^P(2)$–$X^P_A(2)$	2.15(6)
$M^H(2)$–O(9)	1.942(9)	$A^P(1)$–$X^O_A(1)$	2.40(1)	$A^P(2)$–$X^O_A(2)$	2.46(4)
$M^H(2)$–O(5)	1.948(9)	$A^P(1)$–O(4)	2.52(1)	$A^P(2)$–O(9)g	2.49(5)
$M^H(2)$–O(1)	1.952(8)	$A^P(1)$–O(11)e	2.56(1)	$A^P(2)$–O(1)g	2.51(4)
$M^H(2)$–O(13)	1.964(8)	$A^P(1)$–O(13)l	2.62(1)	$A^P(2)$–O(6)o	2.59(5)
$M^H(2)$–$X^P_M(2)$	2.32(1)	$A^P(1)$–O(5)l	2.65(1)	$A^P(2)$–O(14)p	2.61(4)
<$M^H(2)$–φ>	1.987	$A^P(1)$–O(8)m	2.68(1)	$A^P(2)$–O(11)	2.83(3)
		$A^P(1)$–O(2)n	2.69(1)	$A^P(2)$–O(4)f	2.88(3)
		<$A^P(1)$–φ>	2.53	<$A^P(2)$–φ>	2.57
Si(1)–O(1)n	1.593(8)	Si(2)–O(6)	1.580(8)	Si(3)–O(8)	1.599(8)
Si(1)–O(2)n	1.615(9)	Si(2)–O(5)	1.599(8)	Si(3)–O(9)	1.600(9)
Si(1)–O(3)	1.623(9)	Si(2)–O(7)	1.621(9)	Si(3)–O(10)g	1.62(1)
Si(1)–O(4)	1.635(8)	Si(2)–O(4)b	1.625(8)	Si(3)–O(11)g	1.631(8)
<Si(1)–O>	1.617	<Si(2)–O>	1.606	<Si(3)–O>	1.613
Si(4)–O(13)e	1.585(8)	Si(1)–O(4)–Si(2)l	134.5(6)	Short distances	
Si(4)–O(14)e	1.595(9)	Si(3)g–O(11)–Si(4)b	134.6(6)	$A^P(2)$–W	1.65(4)
Si(4)–O(12)	1.61(1)	<Si–O–Si>	134.6	$X^P_A(2)$–W	0.61(4)
Si(4)–O(11)l	1.620(9)				
<Si(4)–O>	1.603				

φ = O, F, OH, H_2O; Symmetry operators: a: x, y–1, z–1; b: x, y–1, z; c: x, y, z–1; d: –x + 1, –y + 1, –z; e: –x + 1, –y + 1, –z + 1; f: –x, –y + 1, –z + 1; g: –x + ½, –y + ½, –z + 1; h: x–1, y, z–1; i: –x, –y, –z; j: x + $^3/_2$, –y + ½, –z + 1; k: x + 1, y, z; l: x, y + 1, z; m: x + ½, y + ½, z; n: x–½, y + ½, z; o: –x, –y, –z + 1; p: –x + 1, –y, –z + 1.

Site-population assignment

There are thirteen cation sites in the crystal structure of zvyaginite: the $M^H(1,2)$, $A^P(1,2)$ and four *Si* sites of the H sheet and five M^O sites of the O sheet; site labelling follows Sokolova (2006).

The two $^{[6]}M^H$ sites in the H sheet have refined site-scattering values of 36.5(3) and 36.0(3) electrons per formula unit (epfu) (Table 7) and we assign all Nb plus some Ti to those two sites. In the O sheet, the refined site-scattering at the $M^O(1)$ site is 21.4(5) epfu (Table 7) and the bond-lengths around this site vary from 1.853 to 2.037 Å (Table 6); we assign the rest of Ti plus minor Al to the $M^O(1)$ site, with a calculated scattering of 21.37 epfu (Table 7).

The two $^{[6]}M^O(2,3)$ sites occur in the O sheet. The refined site-scattering at the $M^O(2)$ site, 2.6(2) epfu, is slightly lower than 2.8(2) epfu at the $M^O(3)$ site (Table 7), and the mean bond-length for the $M^O(2)$ site, 2.483 Å, is slightly longer than 2.479 Å at the $M^O(3)$ site (Table 6) and we assign (0.24 Na + 0.26 □) apfu to the $M^O(2)$ site and (0.18 Na + 0.03 Mn + 0.29 □) apfu to the $M^O(3)$ site, with calculated site-scattering values of 2.64 and 2.73 epfu, respectively (Table 7).

https://doi.org/10.1180/minmag.2017.081.015 Published online by Cambridge University Press

TABLE 7. Refined site-scattering and assigned site-populations for zvyaginite, space group $C\bar{1}$.

Site*		Refined site-scattering (epfu)	Assigned site-population (pfu)	Calculated site-scattering (epfu)	<cation–φ>$_{obs.}$ (Å)	Ideal composition (pfu)
Cations						
$M^H(1)$	[*Nb*(1)]	36.5(3)	0.84 Nb + 0.16 Ti	37.96	1.984	Nb
$M^H(2)$	[*Nb*(2)]	36.0(3)	0.84 Nb + 0.16 Ti	37.96	1.987	Nb
$M^O(1)$	[*Ti*(1,2)]	21.4(5)	0.93 Ti + 0.07 Al	21.37	1.963	Ti
Σ		93.9	1.68 Nb + 1.25 Ti + 0.07 Al	97.29		Nb_2Ti
$M^O(2)$	[*Na*(1)]	2.6(2)	0.24 Na + 0.26 □	2.64	2.483	$□_{0.5}$
$M^O(3)$		2.8(2)	0.18 Na + 0.03 Mn + 0.29 □	2.73	2.479	$□_{0.5}$
$M^O(4)$	[*Zn*(1)]	24.5(2)	0.61 Zn + 0.22 Na + 0.10 Mn + 0.04 Fe^{2+} + 0.03 □	24.26	2.153	Zn
$M^O(5)$	[*Zn*(2)]	14.2(3)	0.48 Na + 0.27 Zn + 0.04 Mn + 0.21 □	14.38	2.42	Na
Σ		44.1	1.12 Na + 0.88 Zn + 0.17 Mn + 0.04 Fe^{2+} + 0.79 □	44.01		NaZn□
$^{[8]}A^P(1)$	[*Na*(2)]	7.9(2)	0.55 Na + 0.09 Ca + 0.36 □	7.85	2.53	Na
$^{[8]}A^P(2)$	[*Na*(3)]	3.0(3)	0.20 Na + 0.04 K + 0.76 □	2.96	2.57	□
Σ		10.9	0.75 Na + 0.09 Ca + 0.04 K + 1.12 □	10.81		Na□
Anions** and H_2O groups						
$X^O_M(1,2)$	[O(6,18)]		2.00 O			O_2
$^{[4,3]}X^O_A(1,2)$	[O(11,12)]		1.11 OH + 0.89 F			$(OH)_2$
$^{[1]}X^P_M(1,2)$	[O(19,20)]		2.00 H_2O			$(H_2O)_2$
$^{[1]}X^P_A(1)$	[O(21)]		1.00 H_2O			H_2O
$^{[1]}X^P_A(2)$	[O(22)]		0.24 H_2O + 0.76 □			□
W			0.76 H_2O + 0.24 □			H_2O
Σ			2.00 O + 1.11 OH + 0.89 F + 4.00 H_2O			$O_2(OH)_2(H_2O)_4$

*Coordination numbers are shown for non-[6]-coordinated cation sites and non-4-coordinated anion sites and H_2O groups; [ ] corresponding sites in Pekov *et al.* (2014); φ = O, F, OH, H_2O; the Ti-dominant general $M^O(1)$ site (this work) corresponds to the two, *Ti*(1) and *Ti*(2), special sites (multiplicity 0.5 apfu) (Pekov *et al.*, 2014); the special $M^O(2)$ and $M^O(3)$ sites (multiplicity 0.5 apfu) occupied mainly by Na at < 50% (this work) correspond to the general *Na*(1) site (Pekov *et al.*, 2014) with 46% occupancy.
**Anions that do not coordinate Si.

The two [8]-coordinated $A^P(1)$ and $A^P(2)$ sites in the H sheet have refined site-scattering values of 7.9(2) and 3.0(3) epfu and mean bond lengths of 2.53 and 2.57 Å (Table 7). We assign (0.55 Na + 0.09 Ca + 0.36 □) pfu to the $A^P(1)$ site and (0.20 Na + 0.04 K + 0.76 □) pfu to the $A^P(2)$ site, with calculated site-scattering values of 7.85 and 2.96 epfu, respectively (Table 7).

We are left with 0.88 Zn + 0.70 Na + 0.14 Mn + 0.04 Fe^{2+} (Table 2) to assign to the [6]-coordinated $M^O(4)$ and $M^O(5)$ sites in the O sheet. The refined site-scattering of 24.5 epfu at the $M^O(4)$ site is higher than that at the $M^O(5)$ site: 14.2 epfu, and the <$M^O(4)$–φ> distance of 2.153 Å [with a calculated aggregate cation r = 0.77 Å, *cf.* $^{[6]}$Zn: r = 0.74 Å,

https://doi.org/10.1180/minmag.2017.081.015 Published online by Cambridge University Press

TABLE 8. Bond-valence values for selected anions* in zvyaginite.

Atom	$M^O(1)$	$M^O(2)$	$M^O(3)$	$M^O(4)$	$M^O(5)$	$M^H(1)$	$M^H(2)$	$A^P(1)$	$A^P(2)$	Σ
Site occ. (%)	100	48	42	97	79	100	100	74	24	
$X^O_M(1)$			0.10	0.30	0.12	1.39				1.91
$X^O_M(2)$		0.10		0.30	0.12		1.36			1.88
$X^O_A(1)$	0.87				0.13 0.13			0.14		1.27
$X^O_A(2)$	0.55			0.24 0.24					0.04	1.07
$X^P_M(1)$						0.38				0.38
$X^P_M(2)$							0.38			0.38
X^P_A (1)								0.33		0.33
X^P_A (2)									0.33	0.33

* Anions which do not coordinate Si; bond-valence parameters (vu) are from Brown (1981); bonds to oxygen were used for Ti [$M^O(1)$]; Na [$M^O(2,3,5)$, $A^P(1,2)$]; Zn [$M^O(4)$] and Nb [$M^H(1,2)$]; site occupancies of cation sites were taken into account for all calculations except for $A^P(2)$ and X^P_A. (2): both sites are occupied at 24% by Na and H_2O, respectively.

Shannon (1976)] is shorter than the <$M^O(5)$–φ> distance of 2.42 Å [with a calculated aggregate cation r = 1.14 Å, *cf.* [6]Na: r = 1.02 Å]. Therefore we assign (0.61 Zn + 0.22 Na + 0.10 Mn + 0.04 Fe^{2+} + 0.03 □) pfu to the $M^O(4)$ site, with a calculated site-scattering of 24.26 epfu and (0.48 Na + 0.27 Zn + 0.04 Mn + 0.21 □) apfu to the $M^O(5)$ site, with a calculated site-scattering of 14.38 epfu (Table 7).

Description of the structure

Cation and anion sites

Here we consider thirteen cation sites, five M^O sites of the O sheet and two M^H, two A^P and four *Si* sites of the H sheet; and eight anion sites: two X^O_M = anion sites at the common vertices of $3M^O$ and M^H polyhedra; two X^O_A = anion sites at the common vertices of $3M^O$ and A^P polyhedra; four $X^P_{(M,A)}$ = anion sites at the apical vertices of two M^H and two A^P polyhedra at the periphery of the TS block; labelling is in accord with Sokolova (2006).

In the O sheet, the $M^O(1)$ site is occupied primarily by Ti with minor Al (Table 7), and it is coordinated by four O atoms and two (OH,F) anions at the X^O_A sites as in epistolite (Figs 4*a*,*b*). The ideal composition of the $M^O(1)$ site is Ti apfu. Note that Pekov *et al.* (2014) reported two *Ti*(1,2) sites, each occupied by 0.5 Ti apfu (Table 3). The □-dominant [6]$M^O(2)$ and [6]$M^O(3)$ sites are less than 50% occupied by Na and Na with minor Mn, respectively (Table 7, Fig. 4*a*). The $M^O(2,3)$ sites are coordinated by six O atoms, with <$M^O(2,3)$–O> = 2.483 and 2.479 Å (Table 6). The ideal composition of the $M^O(2,3)$ sites is $□_{0.5} + □_{0.5}$ = □ pfu (Table 7). Note that Pekov *et al.* (2014) reported one *Na*(1) site, ideally □ pfu (Table 3). The $M^O(4)$ site is occupied primarily by Zn plus Na and Mn with minor Fe^{2+} (Table 7, Fig. 4*a*), and is coordinated by four O atoms and two (OH,F) anions at the X^O_A sites, with <$M^O(4)$–φ> = 2.153 Å (Table 6). The ideal composition of the $M^O(4)$ site is Zn apfu. The $M^O(5)$ site is occupied 79% by Na plus Zn and minor Mn (Table 7, Fig. 4*a*), and it is coordinated by four O atoms and two (OH,F) anions at the X^O_A sites, with <$M^O(5)$–φ> = 2.42 Å (Table 6). The ideal composition of the $M^O(5)$ site is Na apfu. Note that Pekov *et al.* (2014) reported two *Zn*(1,2) sites with ~ 60% occupancy by Zn (Table 3), which ideally give Zn_2 apfu. These *Zn*(1,2) sites correspond to the $M^O(4,5)$ sites (Table 7). The U_{eq} of Zn atoms at the *Zn*(1,2) sites were in the ratio 1:3 (Pekov *et al.*, 2014), inconsistent with equal occupancy of those sites. The U_{eq} of Zn and Na atoms at the $M^O(4)$ and $M^O(5)$ sites are in the ratio 2:3 (this work) and we suggest that the larger cation disorder (and a larger vacancy) at the $M^O(5)$ site results in larger values of displacement parameters.

The sum of the cations at the $M^O(4,5,2,3,1)$ sites gives ideal composition of the O sheet as NaZn□Ti pfu.

In the H sheet, there are four tetrahedrally coordinated *Si*(1–4) sites occupied by Si. There are two Nb-dominant [6]$M^H(1,2)$ sites; each M^H site is coordinated by five O atoms and an H_2O group at

https://doi.org/10.1180/minmag.2017.081.015 Published online by Cambridge University Press

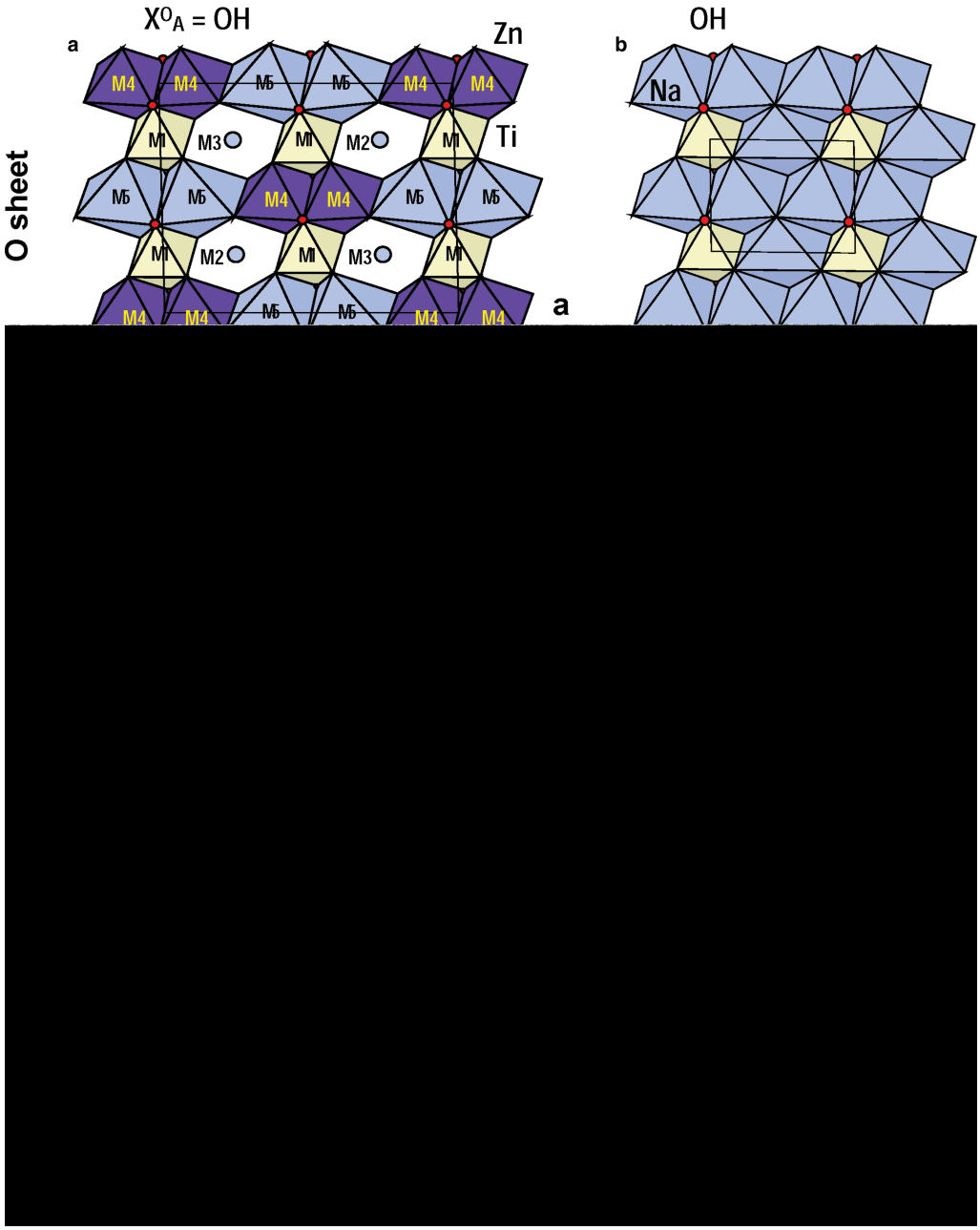

FIG. 4. The details of the TS block: the O sheet of Na-dominant $M^{O}(5)$ octahedra, Ti-dominant $M^{O}(1)$ octahedra and Zn-dominant $M^{O}(4)$ octahedra [$M^{O}(2,3)$ sites are occupied by Na at less than 50%] in zvyaginite (*a*) and the O sheet of Na and Ti octahedra in epistolite (*b*); the H sheet of Si_2O_7 groups, Nb-dominant M^{H} octahedra and [8]-coordinated Na-dominant $A^{P}(1)$ polyhedra (64% occupancy) [the $A^{P}(2)$ site is occupied by Na at 24%] in zvyaginite (*c*) and the H sheet of Si_2O_7 groups, Nb-dominant octahedra and [8]-coordinated Na-dominant polyhedra (59% occupancy) in epistolite (*d*); the TS block in zvyaginite (*e*) and epistolite (*f*). Si tetrahedra are orange, Nb-dominant and Ti-dominant octahedra are yellow; Na-dominant and Zn-dominant polyhedra are navy blue and purple, OH groups at the X^{O}_{A} sites are shown as medium red spheres, H_2O groups at the X^{P} and *W* sites are shown as large red spheres, cation sites with < 50% occupancy by Na are shown as navy blue spheres. The unit cell is shown by thin black lines in (*a–d*).

https://doi.org/10.1180/minmag.2017.081.015 Published online by Cambridge University Press

the X^{P}_{M} site as in epistolite (Figs 4*c*,*d*). The M^{H}(1,2) sites ideally give Nb_2 apfu. Note that the U_{eq} of Nb atoms at the M^{H}(1,2) sites are in the ratio 1:1. The two $^{[8]}A^{P}$(1,2) sites are occupied 64% by Na and minor Ca and 24% by Na and minor K, respectively; ideally they give Na□ pfu (Table 7). Each A^{P} site is coordinated by six O atoms, an OH group at the X^{O}_{A} site and an H_2O group at the X^{P}_{A} site, as in epistolite (Table 6, Figs 4*c*,*d*). The ideal composition of the $A^{P} + M^{H}$ sites is Na□Nb_2 pfu.

We write the cation part of the TS block as the sum of cations of the 2H and O sheets: ideally Na□Nb_2NaZn□Ti pfu, with a total charge of 18^{+}.

The four Si(1–4) atoms and fourteen O(1–14) atoms (Table 5) that coordinate the Si atoms give $(Si_2O_7)_2$ pfu. Anions at the X^{O}_{M}(1 and 2) sites receive bond valences from four cations: M^{O}(3 and 2), M^{O}(4), M^{O}(5) and M^{H}, with total bond-valence sums of 1.91 and 1.88 vu (valence units) (Table 8) and they are O atoms, giving O_2 apfu (Table 7). Anions at the X^{O}_{A} (1 and 2) sites receive bond valences from four cations: M^{O}(1), $2M^{O}$(5 and 4) and A^{P}(1 and 2), with total bond-valence sums of 1.27 and 1.07 vu (Table 8, Fig. 4*a*) and we assign monovalent anions to these two sites: 1.11 OH + 0.89 F, ideally $(OH)_2$ pfu (Table 7). The four $X^{P}_{(M,A)}$ sites are occupied by H_2O groups (Tables 8, Fig. 4*c*) as in epistolite (Fig. 4*d*) (Sokolova and Hawthorne, 2004). The X^{P}_{M}(1,2) and X^{P}_{A}(1) sites are occupied by H_2O at 100% and the X^{P}_{A}(2) site at 24% (Tables 7). There is a new *W* site (when compared to epistolite) which is occupied by H_2O groups at 76% (Tables 5,7). The four $X^{P}_{(M,A)}$ sites and the *W* site give $(H_2O)_4$ pfu (Table 7). The anions and H_2O groups sum as follows: $(Si_2O_7)_2$ [O(1–14)] + O_2 + $(OH)_2$ + $(H_2O)_4$ = $(Si_2O_7)_2O_2(OH)_2(H_2O)_4$ pfu, with a total charge of 18^{-}. We write ideal structural formula of zvyaginite as the sum of cation and anion parts: Na□Nb_2NaZn□Ti + $(Si_2O_7)_2O_2(OH)_2(H_2O)_4$ = Na□Nb_2NaZn□Ti$(Si_2O_7)_2O_2(OH)_2(H_2O)_4$, $Z = 4$. A short form of the ideal structural formula is $Na_2ZnTiNb_2(Si_2O_7)_2O_2(OH)_2(H_2O)_4$.

Structure topology of zvyaginite

The main structural unit in the crystal structure of zvyaginite is a TS block that consists of HOH sheets. The O sheet is composed of Ti-dominant M^{O}(1), Zn-dominant M^{O}(4) and Na-dominant M^{O}(5) octahedra, with □-dominant M^{O}(2,3) sites occupied mainly by Na at <50% (Fig. 4*a*). In epistolite, Ti-dominant and Na-dominant octahedra constitute the O sheet (Fig. 4*b*). The ideal compositions of the O sheet in zvyaginite, $[Na□ZnTiO_2(OH)_2]^{1+}$ pfu, and epistolite, $[Na_3TiO_2(OH)_2]^{1+}$ apfu (Sokolova and Hawthorne, 2004) are related by the following substitution: $(Na^{+}_{2})_{epi} \leftrightarrow Zn^{2+}_{zvy} + □_{zvy}$.

In zvyaginite, the H sheet is built of Si_2O_7 groups, Nb-dominant $^{[6]}M^{H}$ and Na-dominant $^{[8]}A^{P}$(1) polyhedra, with the □-dominant $^{[8]}A^{P}$(2) site occupied mainly by Na at 24% (Fig. 4*c*). In epistolite, there is only one $^{[8]}A^{P}$ site occupied mainly by Na at 59% (Fig. 4*d*) and Sokolova and Hawthorne (2004) wrote its composition as (Na□) pfu, with cations of the two H sheets summing to (Na□)Nb_2 pfu. Hence ideal compositions of the H sheets in zvyaginite, $[Na□Nb_2(Si_2O_7)_2(H_2O)_4]^{1-}$ pfu, and epistolite, $[(Na□)Nb_2(Si_2O_7)_2(H_2O)_4]^{1-}$ pfu are quantitatively identical but differ in the order of Na and □ over two A^{P}sites in zvyaginite and the disorder of Na and □ within one A^{P}site in epistolite.

In zvyaginite and epistolite, the topology of the TS block is as in the lamprophyllite group of the TS-block minerals where Ti (+ Nb + Fe^{3+} + Mg) = 3 apfu per $(Si_2O_7)_2$: two H sheets connect to the O sheet such that two Si_2O_7 groups link to the *trans* edges of a Ti [M^{O}(1)] octahedron of the O sheet (Figs 4*e*,*f*). In the crystal structures of zvyaginite and epistolite, TS blocks parallel to (001) link via hydrogen bonds between H_2O groups at apical vertices [$X^{P}_{(M,A)}$ sites] of M^{H} and A^{P} polyhedra (Fig. 5*a*,*b*).

Figure 6 shows H_2O groups forming a ribbon along **a**. Analogous ribbons of H_2O groups occur in epistolite (Sokolova and Hawthorne, 2004) and a seidozerite-supergroup mineral murmanite, $Na_4Ti_4(Si_2O_7)_2O_4(H_2O)_4$ (Cámara *et al.*, 2008). In zvyaginite, there is disorder of Na and □ at the A^{P}(2) site and H_2O and □ at the *W* and X^{P}_{A}(2) sites, where Na at the A^{P}(2) site (24% occupancy) and an H_2O group at the X^{P}_{A}(2) site (24% occupancy) occur at short distances from an H_2O group at the *W* site (76% occupancy), 1.65 and 0.61 Å, respectively (Table 6, Fig. 4*c*). We suggest that two short-range-order arrangements around the A^{P}(2) site are possible: (1) the A^{P}(2) and X^{P}_{A}(2) sites are locally occupied by Na and H_2O and the *W* site is vacant; (2) the A^{P}(2) and X^{P}_{A}(2) sites are locally vacant and the *W* site is occupied by H_2O (Fig. 6).

We conclude that (1) the general topology of the crystal structure of zvyaginite described above is in accord with Pekov *et al.* (2014); (2) the stereochemistry of Ti, Zn and Na in the TS block, especially for the O sheet, is different from that reported by Pekov *et al.* (2014); (3) doubling of the t_1 and t_2 translations of zvyaginite, $a_{zvy} = 10.769$, $b_{zvy} = 14.276$ Å,

https://doi.org/10.1180/minmag.2017.081.015 Published online by Cambridge University Press

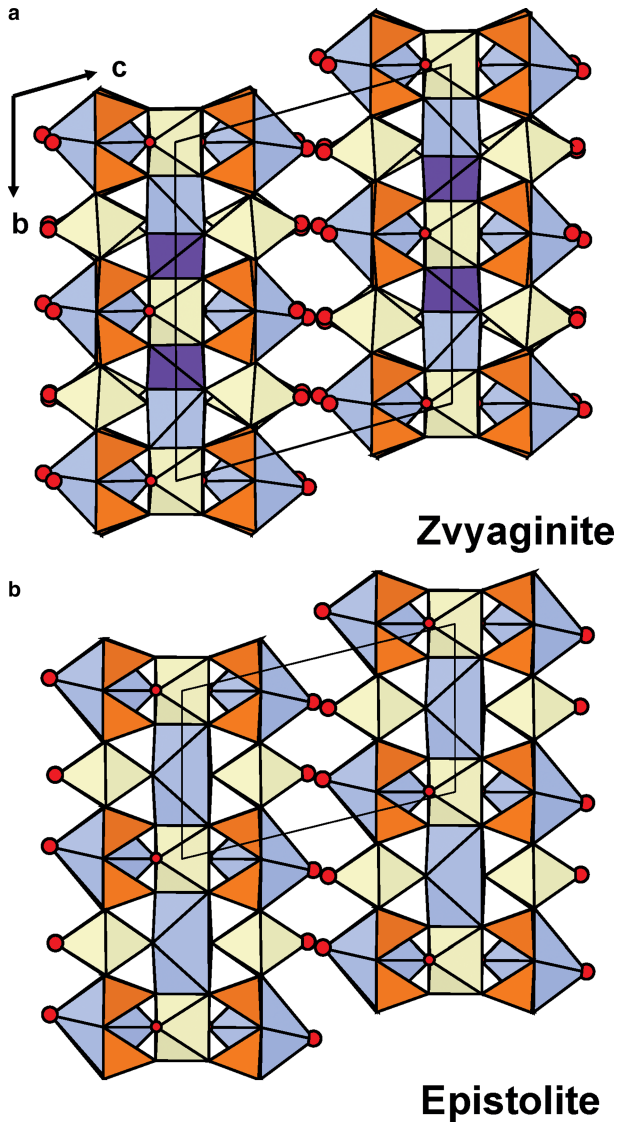

FIG. 5. A general view of the crystal structures of zvyaginite (*a*) and epistolite (*b*), cations (and polyhedra) at sites with occupancy less than 50% are not shown. Legend as in Fig. 4.

relative to those of epistolite: $a_{epi} = 5.460$, $b_{epi} = 7.170$ Å (Fig. 4*b*), is due to order of Zn and Na along **a** ($\mathbf{t_1}$) and **b** ($\mathbf{t_2}$) in the O sheet of zvyaginite.

The ideal structural formula of zvyaginite

Above, we wrote the ideal structural formula of zvyaginite based on the occupancies of the cation and anion sites. Here, we write the ideal structural formula of zvyaginite in accord with Sokolova (2006); we use the general structural formula of the lamprophyllite-group mineral epistolite: $A^P_2M^H_2M^O_4(Si_2O_7)_2(X^O_M)_2(X^O_A)_2(X^P_{M,A})_4$ where A^P are cations at the peripheral (*P*) sites; M^H and M^O are cations of the H and O sheets; X^O are anions of the O sheet; X^P_M and X^P_A are apical anions of the M^H and A^P cations at the periphery of the TS block. In zvyaginite, $A^P_2 = A^P(1) + A^P(2) = Na + \square = Na\square$; $M^H_2 = M^H(2) + M^H(1) = Nb_2$; $M^O_4 = NaZn\square Ti$;

https://doi.org/10.1180/minmag.2017.081.015 Published online by Cambridge University Press

$(X^{O}_{M})_2 = O_2$; $(X^{O}_{A})_2 = (OH)_2$; $(X^{P}_{M,A})_4 = (X^{P}_{M})_2 + X^{P}_{A} + W = (H_2O)_2 + H_2O + H_2O = (H_2O)_4$. Hence, we write the ideal composition of the TS block in zvyaginite as follows:

$$^{A^P}[Na\square]^{M^H}[Nb_2]^{M^O}[NaZn\square Ti](Si_2O_7)_2{}^{X^O}[O_2(OH)_2]\ ^{X^P_{(M,A)}}[(H_2O)_4]$$
$$= Na\square Nb_2NaZn\square Ti(Si_2O_7)_2O_2(OH)_2(H_2O)_4,$$
$$Z = 4.$$

Summary

(1) Electron-microprobe analysis of zvyaginite from the type locality, Mt. Malyi Punkaruaiv, Lovozero alkaline massif, Kola Peninsula, Russia gave a higher Na_2O content than that reported previously: 7.10 *vs.* 4.74 wt.% (Pekov *et al.*, 2014). The empirical and ideal formulae of zvyaginite have been revised as follows: $(Na_{0.75}Ca_{0.09}K_{0.04}\square_{1.12})_{\Sigma 2}$ $(Na_{1.12}Zn_{0.88}Mn_{0.17}Fe^{2+}_{0.04}\square_{0.79})_{\Sigma 3}(Nb_{1.68}Ti_{1.25}Al_{0.07})_{\Sigma 3}(Si_{4.03}O_{14})O_2$ $[(OH)_{1.11}F_{0.89}]_{\Sigma 2}(H_2O)_4$ and $Na_2ZnTiNb_2(Si_2O_7)_2O_2(OH)_2(H_2O)_4$, $Z = 4$ [*cf.* idealized formula of Pekov *et al.* (2014): $NaZnNb_2Ti(Si_2O_7)_2O(OH)_3(H_2O)_4$, $Z = 2$].

(2) The crystal structure of zvyaginite has been revised: space group $C\bar{1}$, $a = 10.769(2)$, $b = 14.276(3)$, $c = 12.101(2)$ Å, $\alpha = 105.45(3)$, $\beta = 95.17(3)$, $\gamma = 90.04(3)°$, $V = 1785.3(3.2)$ Å^3, $R_1 = 9.23\%$, $Z = 4$. The general topology of the crystal structure is in accord with Pekov *et al.* (2014): it is an array of TS blocks connected via hydrogen bonds between H_2O groups. However the stereochemistry of the TS block is different from that of Pekov *et al.* (2014): the choice of a new origin in the crystal structure of zvyaginite reveals order of Zn and Na in the O sheet of the TS block of the composition $[NaZn\square TiO_2(OH)_2]^{1+}$ and order of Na and $\square$ in the two H sheets of the composition $[Na\square Nb_2(Si_2O_7)_2(H_2O)_4]^{1-}$. The structure-refinement results are in accord with the chemical analysis.

(3) Zvyaginite, ideally $Na\square Nb_2NaZn\square Ti(Si_2O_7)_2O_2(OH)_2(H_2O)_4$, is a TS-block mineral of the lamprophyllite group (seidozerite supergroup) where $Ti + Nb + Fe^{3+} + Mg = 3$ apfu. The crystal structure of zvyaginite is of the same topology as that of epistolite, $(Na\square)Nb_2Na_3Ti(Si_2O_7)_2O_2(OH)_2(H_2O)_4$. Zvyaginite is a Zn-bearing and Na-poor analogue of epistolite.

(4) Epistolite and zvyaginite are related by the following substitution in the O sheet of the TS-block: $(Na^+_2)_{epi} \leftrightarrow Zn^{2+}_{zvy} + \square_{zvy}$. The doubling of the t_1 and t_2 translations of zvyaginite, $a_{zvy} = 10.769$, $b_{zvy} = 14.276$ Å, relative to those of epistolite: $a_{epi} = 5.460$, $b_{epi} = 7.170$ Å, is due to the order of Zn and Na along **a** ($\mathbf{t_1}$) and **b** ($\mathbf{t_2}$) in the O sheet of zvyaginite.

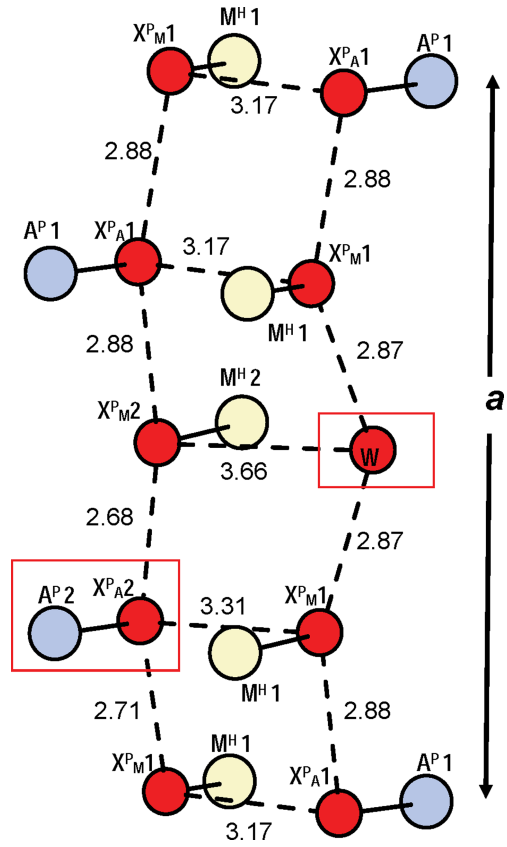

FIG. 6. A general scheme of possible hydrogen bonding in zvyaginite. O atoms of H_2O groups at the X^P and W sites are shown as large red spheres, [8]-coordinated Na atoms at the A^P sites are shown as blue spheres and [6]-coordinated Nb atoms at the M^H sites are shown as yellow spheres; bonds Nb–O(H_2O) and Na–O(H_2O) are shown as solid black lines; possible directions of hydrogen bonds are shown as dashed black lines and their lengths are given in Å. Red rectangles show possible short-range-order arrangements around the $A^P(2)$ site: (*left*) SRO 24%: $A^P(2) = Na$, $X^P(2) = H_2O$, $W = \square$; (*right*) SRO 76%: $A^P(2) = \square$, $X^P(2) = \square$, $W = H_2O$.

(5) The TEM investigation revealed a band structure characterized by the alternation of defect-free bands and defect-rich domains along the <001> direction. The defect-bearing bands, in turn, exhibit interleaving of {001} lamellae extended many hundreds of nanometres along the <110> direction, a few tens of nanometres along the <001> and very few tens of nanometres along the <$\bar{1}$10> direction.

https://doi.org/10.1180/minmag.2017.081.015 Published online by Cambridge University Press

Khomyakov (1995) coined the name transformation minerals for vuonnemite, ideally $Na_6Na_2Nb_2Na_3Ti(Si_2O_7)_2(PO_4)_2O_2(OF)$ (Ercit *et al.*, 1998) and epistolite, ideally $(Na\square)Nb_2Na_3Ti(Si_2O_7)_2O_2(OH)_2(H_2O)_4$, meaning that epistolite is formed by ion-exchange from vuonnemite, a precursor mineral of related structure. The interleaving of well-crystalline zvyaginite with lamellae of poor crystallinity and undulating lattice planes supports the idea of Pekov *et al.* (2014) that epistolite and zvyaginite are transformation minerals, too.

Acknowledgements

We are grateful to an anonymous reviewer and Associate Editor Peter Leverett for useful comments. We thank Mark A. Cooper for collection of single-crystal X-ray data for three zvyaginite crystals. ES acknowledges financial support by a Canada Research Chair in Crystallography and Mineralogy to FCH. FCH acknowledges support by a Canada Research Chair in Crystallography and Mineralogy and by a Discovery Grant from the Natural Sciences and Engineering Research Council of Canada, and by Innovation Grants from the Canada Foundation for Innovation.

References

Aksenov, S.M., Rastsvetaeva, R.K. and Chukanov, N.V. (2014) The crystal structure of emmerichite $Ba_2Na_3Fe^{3+}Ti_2(Si_2O_7)_2O_2F_2$, a new lamprophyllite-group mineral. *Zeitschrift für Kristallographie*, **229**, 1–7.

Andrade, M.B., Yang, H., Downs, R.T., Färber, G., Contreira Filho, R.R., Evans, S.H., Loehn, C.W. and Schumer, B.N. (2017) Fluorlamprophyllite, $Na_3(SrNa)Ti_3(Si_2O_7)O_2F_2$, a new mineral from Poços de Caldas alkaline massif, Morro do Serrote, Mines Gerais, Brazil. *Mineralogical Magazine*, https://doi.org/10.1180/minmag.2017.081.027

Brown, I.D. (1981) The bond-valence method: an empirical approach to chemical structure and bonding. Pp. 1–30 in: *Structure and Bonding in Crystals II* (M. O'Keeffe and A. Navrotsky, editors). Academic Press, New York.

Cámara, F. and Sokolova, E. (2007) From structure topology to chemical composition. VI. Titanium silicates: the crystal structure and crystal chemistry of bornemanite, a group III Ti-disilicate mineral. *Mineralogical Magazine*, **71**, 593–610.

Cámara, F. and Sokolova, E. (2009) From structure topology to chemical composition. X. Titanium silicates: the crystal structure and crystal chemistry of nechelyustovite, a group III Ti-disilicate mineral. *Mineralogical Magazine*, **73**, 887–897.

Cámara, F., Sokolova, E., Hawthorne, F.C. and Abdu, Y. (2008) From structure topology to chemical composition. IX. Titanium silicates: revision of the crystal chemistry of lomonosovite and murmanite, Group-IV minerals. *Mineralogical Magazine*, **72**, 1207–1228.

Cámara, F., Sokolova, E. and Hawthorne, F.C. (2012) Kazanskyite, $BaTiNbNa_3Ti(Si_2O_7)_2O_2(OH)_2(H_2O)_4$, a Group-III Ti-disilicate mineral from the Khibiny alkaline massif, Kola Peninsula, Russia: description and crystal structure. *Mineralogical Magazine*, **76**, 473–492.

Cámara, F., Sokolova, E., Abdu, Y.A. and Hawthorne, F.C. (2014) Saamite, $Ba\square TiNbNa_3Ti(Si_2O_7)_2O_2(OH)_2(H_2O)_2$, a Group-III Ti-disilicate mineral from the Khibiny alkaline massif, Kola Peninsula, Russia: description and crystal structure. *The Canadian Mineralogist*, **52**, 745–761.

Chukanov, N.V., Pekov, I.V., Rastsvetaeva, R.K., Aksenov, S.M., Zadov, A.E., Van, K.V., Blass, G., Schüller, W. and Ternes, B. (2012) Lileyite, $Ba_2(Na,Fe,Ca)_3MgTi_2(Si_2O_7)_2O_2F_2$, a new lamprophyllite-group mineral from the Eifel volcanic area, Germany. *European Journal of Mineralogy*, **24**, 181–188.

Ercit, T.S., Cooper, M.A. and Hawthorne, F.C. (1998) The crystal structure of vuonnemite, $Na_{11}Ti^{4+}Nb_2(Si_2O_7)_2(PO_4)_2O_3(F,OH)$, a phosphate-bearing sorosilicate of the lomonosovite group. *The Canadian Mineralogist*, **37**, 1311–1320.

Khomyakov, A.P. (1995) *Mineralogy of Hyperagpaitic Alkaline Rocks*. Clarendon Press, Oxford, UK.

Krivovichev, S.V., Armbruster, T., Yakovenchuk, V.N., Pakhomovsky, Ya.A. and Men'shikov, Yu. P. (2003) Crystal structures of lamprophyllite-2*M* and lamprophyllite-2*O* from the Lovozero alkaline massif, Kola peninsula, Russia. *European Journal of Mineralogy*, **15**, 711–718.

Lykova, I.S., Pekov, I.V., Zubkova, N.V., Yapaskurt, V.O., Chervonnaya, N.A., Zolotarev, A.A. and Giester, G. (2015) Crystal chemistry of cation-exchanged forms of epistolite-group minerals. Part II. Vigrishinite and Zn-exchanged murmanite. *European Journal of Mineralogy*, **27**, 669–682.

Pekov, I.V., Britvin, S.N., Zubkova, N.V., Chukanov, N.V., Bryzgalov, I.A., Lykova, I.S., Belakovskiy, D.I. and Pushcharovsky, D.Yu. (2013) Vigrishinite, $Zn_2Ti_{4-x}Si_4O_{14}(OH,H_2O,\square)_8$, a new mineral from the Lovozero alkaline complex, Kola Peninsula, Russia. *Geology of Ore Deposits*, **55**, 575–586.

Pekov, I.V., Lykova, I.S., Chukanov, N.V., Yapaskurt, V. O., Belakovskiy, D.I., Zolotarev Jr, A.A. and Zubkova, N.V. (2014) Zvyaginite, $NaZnNb_2Ti(Si_2O_7)_2O(OH,F)_3(H_2O)_{4+x}$ ($x < 1$), a new mineral of the epistolite group from the Lovozero alkaline pluton, Kola Peninsula, Russia. *Geology of Ore Deposits*, **56**, 644–656.

https://doi.org/10.1180/minmag.2017.081.015 Published online by Cambridge University Press

Pouchou, J.L. and Pichoir, F. (1985) "PAP" φ(ρZ) procedure for improved quantitative microanalysis. Pp. 104–106 in: *Microbeam Analysis* (J.T. Armstrong, editor). San Francisco Press, San Francisco, California, USA.

Rastsvetaeva, R.K. and Chukanov, N.V. (1999) Crystal structure of a new high-barium analogue of lamprophyllite with a primitive unit cell. *Doklady Chemistry*, **368**, 228–231.

Shannon, R.D. (1976) Revised effective ionic radii and systematic studies of interatomic distances in halides and chalcogenides. *Acta Crystallographica*, **A32**, 751–767.

Sheldrick, G.M. (2008) A short history of SHELX. *Acta Crystallographica*, **A64**, 112–122.

Sokolova, E. (2006) From structure topology to chemical composition. I. Structural hierarchy and stereochemistry in titanium disilicate minerals. *The Canadian Mineralogist*, **44**, 1273–1330.

Sokolova, E. and Cámara, F. (2007) From structure topology to chemical composition. II. Titanium silicates: revision of the crystal structure and chemical formula of delindeite. *The Canadian Mineralogist*, **45**, 1247–1261.

Sokolova, E. and Cámara, F. (2008) From structure topology to chemical composition. III. Titanium silicates: crystal chemistry of barytolamprophyllite. *The Canadian Mineralogist*, **46**, 403–412.

Sokolova, E. and Cámara, F. (2013) From structure topology to chemical composition. XVI. New developments in the crystal chemistry and prediction of new structure topologies for titanium disilicate minerals with the TS block. *The Canadian Mineralogist*, **51**, 861–891.

Sokolova, E. and Cámara, F. (2016) From structure topology to chemical composition. XXI. Understanding the crystal chemistry of barium in TS-block minerals. *The Canadian Mineralogist*, **54**, 79–95.

Sokolova, E. and Cámara, F. (2017) The seidozerite supergroup of TS-block minerals: nomenclature and classification, with change of the following names rinkite to rinkite-(Ce), mosandrite to mosandrite-(Ce), hainite to hainite-(Y) and innelite-1*T* to innelite-1*A*. *Mineralogical Magazine*, **81**, 1457–1484.

Sokolova, E. and Hawthorne, F.C. (2004) The crystal chemistry of epistolite. *The Canadian Mineralogist*, **42**, 797–806.

Sokolova, E. and Hawthorne, F.C. (2008) From structure topology to chemical composition. IV. Titanium silicates: the orthorhombic polytype of nabalamprophyllite from Lovozero massif, Kola Peninsula, Russia. *The Canadian Mineralogist*, **46**, 1323–1331.

Sokolova, E., Cámara, F. and Hawthorne, F.C. (2011) From structure topology to chemical composition. XI. Titanium silicates: crystal structures of innelite-1*T* and innelite-2*M* from the Inagli massif, Yakutia, Russia and the crystal chemistry of innelite. *Mineralogical Magazine*, **75**, 2495–2518.

Wilson, A.J.C. (editor) (1992) *International Tables for Crystallography. Volume C: Mathematical, physical and chemical tables*. Kluwer Academic Publishers, Dordrecht, The Netherlands.

https://doi.org/10.1180/minmag.2017.081.015 Published online by Cambridge University Press